Acta Pharmaceutica Sinica B 2020;10(12):2374–2383

Chinese Pharmaceutical Association
Institute of Materia Medica, Chinese Academy of Medical Sciences

Acta Pharmaceutica Sinica B

www.elsevier.com/locate/apsb
www.sciencedirect.com

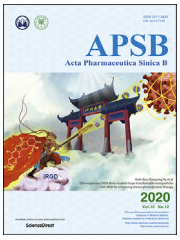

ORIGINAL ARTICLE

Selectively enhancing radiosensitivity of cancer cells *via in situ* enzyme-instructed peptide self-assembly

Yang Gao[a,†], Jie Gao[a,†], Ganen Mu[a], Yumin Zhang[a], Fan Huang[a], Wenxue Zhang[b], Chunhua Ren[a,*], Cuihong Yang[a,*], Jianfeng Liu[a,*]

[a]*Tianjin Key Laboratory of Radiation Medicine and Molecular Nuclear Medicine, Institute of Radiation Medicine, Chinese Academy of Medical Sciences & Peking Union Medical College, Tianjin 300192, China*
[b]*Radiation Oncology Department, Tianjin Medical University General Hospital, Tianjin 300052, China*

Received 25 March 2020; received in revised form 20 May 2020; accepted 23 June 2020

KEY WORDS

In situ enzyme-instructed self-assembly (EISA);
Pre-assembly;
Alkaline phosphatase (ALP);
Peptide;
Cancer radiotherapy;
Nanofiber;
Histone deacetylases inhibitor (HDACI);
Radiosensitizer

Abstract The radiotherapy modulators used in clinic have disadvantages of high toxicity and low selectivity. For the first time, we used the *in situ* enzyme-instructed self-assembly (EISA) of a peptide derivative (Nap-G^{D}F^{D}FpYSV) to selectively enhance the sensitivity of cancer cells with high alkaline phosphatase (ALP) expression to ionizing radiation (IR). Compared with the *in vitro* pre-assembled control formed by the same molecule, assemblies formed by *in situ* EISA in cells greatly sensitized the ALP-high-expressing cancer cells to γ-rays, with a remarkable sensitizer enhancement ratio. Our results indicated that the enhancement was a result of fixing DNA damage, arresting cell cycles and inducing cell apoptosis. Interestingly, *in vitro* pre-formed assemblies mainly localized in the lysosomes after incubating with cells, while the assemblies formed *via in situ* EISA scattered in the cell cytosol. The accumulation of these molecules in cells could not be inhibited by endocytosis inhibitors. We believed that this molecule entered cancer cells by diffusion and then *in situ* self-assembled to form nanofibers under the catalysis of endogenous ALP. This study provides a successful example to utilize intracellular *in situ* EISA of small molecules to develop selective tumor radiosensitizers.

*Corresponding authors.
E-mail addresses: renchunhua@irm-cams.ac.cn (Chunhua Ren), yangcuihong@irm-cams.ac.cn (Cuihong Yang), liujianfeng@irm-cams.ac.cn (Jianfeng Liu).
[†]These authors made equal contributions to this work.
Peer review under responsibility of Chinese Pharmaceutical Association and Institute of Materia Medica, Chinese Academy of Medical Sciences.

https://doi.org/10.1016/j.apsb.2020.07.022

1. Introduction

Radiotherapy, surgery, chemotherapy and immunotherapy are the four prevalent approaches for cancer treatments. It was estimated that more than half of the patients with cancer need to receive radiotherapy alone or in combination with other methods in the course of treatment[1,2]. The disadvantages of radiotherapy include damage to surrounding tissues, severe side effects and strong resistance readily developed by cancer cells due to hypoxic microenvironment and intracellular antioxidant systems[3]. Thus, there is always an unmet demand for safer and more effective radiosensitization methods to improve the efficiency of radiotherapy. The continuous development of cancer biology has advanced enormously our understanding of radiosensitivity. To further widen the therapeutic window, a wide range of biological and chemical methods are employed in order to enhance tumor radiosensitization[4–7]. In the past two decades, the rapid development of nanoscience has brought great opportunities for improving tumor radiosensitization[8,9]. One strategy is to enhance the intracellular deposition of radiation energy using high Z nanomaterials, including Au-, gadolinium (Gd)- and bismuth (Bi)-based nanoparticles. Particularly, the utilization of gold nanoparticles (AuNPs) as radiosensitizers has shown great promise[10,11]. Recently, a large number of new nano-radiosensitizers have been reported, for example, nanomaterials capable of promoting reactive oxygen species (ROS) generation, regulating tumor microenvironment, and affecting tumor cell cycle as well as signal transduction[12]. Unfortunately, few nanoparticle-based radiosensitizers are under clinical trials and no nano-radiosensitizers are commercially available[13]. The properties of nano-particles including low bioavailability, tissue toxicity and nonspecific targeting are the main obstacles to the successful development of nano-radiosensitizers for clinical applications[14]. To improve bioavailability and tumor selectivity are the focuses of the design and development of superior tumor radiosensitizers.

With the advances of synthesis and modification methods, biocompatible peptide-based materials have been widely used in fields of regenerative medicine, bioimaging, cancer treatment and anti-bacteria[15–17]. Most recently, nanomaterials based on supramolecular self-assembled peptides have emerged in the field of radiosensitization. For instance, Xu et al.[18] have designed and developed a curcumin-based supramolecular nanofiber, which could significantly enhance the sensitivity of colorectal cancer cells to ionizing radiation (IR). The self-assembly of this peptide is triggered by glutathione (GSH) highly expressed in tumor cells. Since properties and functions of pre-assembled nanomaterials are somewhat compromised under the complicated physiological conditions, the "*in situ* self-assembly" strategy has been proposed and developed in the past several years[19]. *In situ* self-assembly of the peptide is the generation of aggregates or assemblies at a specific site where the triggers are. Such triggers include enzymes, pH change, and ligand−receptor interactions. The *in situ* assembly only takes place in a specific target site and maintains stable morphology and biochemical properties at the sites of effect. Thus, *in situ* self-assembly renders nanomaterials better selectivity, leading to superior performance. Xu and co-workers[20] pioneered the enzyme-instructed self-assembly (EISA) of peptides in/on living cells to selectively kill cancer cells and overcome multidrug resistance. Wang and co-workers[21] developed *in vivo* self-assembly of responsive peptide derivatives for cancer theranostics. Our group also designed a peptide probe for bacteria detection based on self-assembly mediated by specific binding of vancomycin to D-Ala-D-Ala on the cell wall of Gram-positive bacteria[22]. These smart strategies have also been used in intracellular enzyme activity profiling[23,24], disease progression monitoring[25], biomedical imaging and disease treatment[26].

Histone deacetylases (HDACs) are a family of enzyme associated with chromatin conformation regulation, protein–DNA interaction and DNA transcription and play important roles in a variety of pathophysiological conditions. HDAC inhibitors (HDACIs), which inhibit HDACs activity by reducing histone deacetylation, have been drawing a lot of attention as a new class of anticancer drugs[27–29]. Studies have also shown that HDACIs can change the acetylation level of proteins other than histone to regulate cellular processes associated with cell proliferation, differentiation and survival[30]. However, the HDACIs approved by U. S. Food and Drug Administration (FDA), such as vorinostat and romidepsin, do not achieve satisfactory clinical results due to their poor pharmacodynamic properties[31]. As histone acetylation plays a critical role in regulating chromatin structure and gene expression and is closely related to the radioresponse of tumor radiotherapy, HDACIs have great potential in improving the efficacy of radiotherapy[32]. With the rapid development of molecular radiobiology, it has been found that HDACIs can enhance the sensitivity of tumor cells to radiotherapy by activating stress response, regulating cell cycle, impeding DNA repair, and inducing apoptosis and other signal transduction pathways[5,33]. Due to its high toxicity and lacking selectivity, HDACIs may cause unpredictable side effects[34,35].

Inspired by the work mentioned above, we reasoned that *in-situ* self-assembly might be a feasible strategy to develop new and efficient HDACI-based radiosensitizers. Tri-peptide Tyr-Ser-Val (YSV) has proved to be an HDACI and its tumor inhibition efficacy was significantly improved after being conjugated with self-assembling peptides[36–38]. To the best of our knowledge, the construction of radiosensitizer by *in situ* assembly of peptides in the tumor cell has rarely been reported. In this study, we reported the design and development of an *in situ* self-assembling peptide Nap-G^{D}F^{D}FpYSV (**1P**), capable of assembling into nanofibers by the catalysis of alkaline phosphatase (ALP). As a radiosensitizer, this peptide-based radiosensitizer is able to enhance the radiotherapy treatment on HeLa cells (Scheme 1A). To visualize the ALP-instructed assembly of **1P** in the cellular context, 7-nitro-1,2,3-benzoxadiazole (NBD) is used as an N-terminal capping group to synthesize NBD-^{D}F^{D}FpYSV (**2P**, shown in Scheme 1A) as a **1P** analog. Compared with the pre-assembled radiosensitizer (**1P** + ALP), which was catalyzed by ALP in advance, the *in situ* self-assembling peptide (**1P**) exhibits higher radiosensitization efficiency indicated by an enhanced inhibition of HDAC (Scheme 1B). The combination of EISA and HDACI provides an unprecedented way not only to achieve a better selectivity in targeting cancer cells with high expression of specific enzymes, but also leads to an improved therapeutic effect by reducing off-target effect.

2. Materials and methods

2.1. Materials

Fmoc-amino acids and 2-chlorotrityl chloride resin were purchased from GL Biochem (Shanghai, China). β-Alanine, 4-chloro-7-nitro-1,2,3-benzoxadiazole (NBD-Cl), crystal violet, bovine serum albumin (BSA), DAPI, propidium iodide (PI), L-

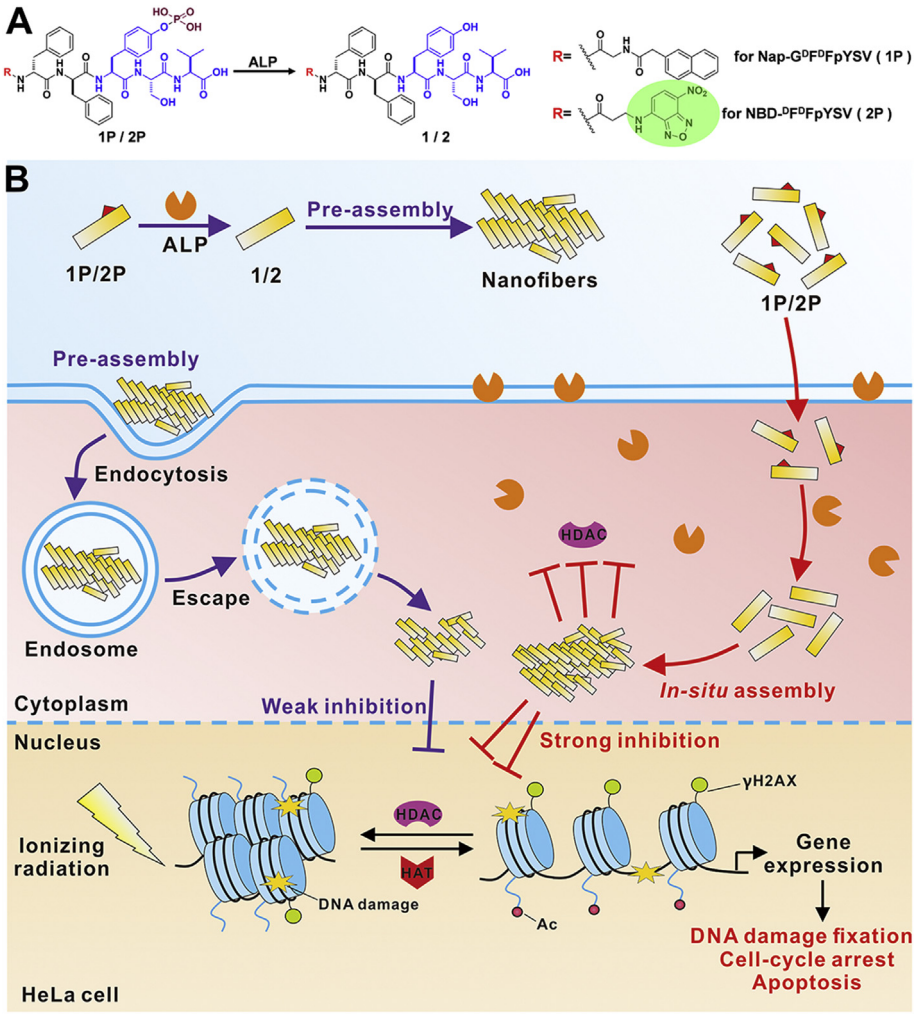

Scheme 1 (A) The molecular structure of **1P** and **2P** and the enzyme-instructed conversion of **1P** and **2P** by alkaline phosphatase (ALP). (B) The schematic illustration of *in situ* EISA of **1P** and **2P** and the plausible mechanism for the enhancement of cancer cells sensitivity to IR.

phenylalanine and other chemical reagents were bought from Solarbio Science & Technology Co., Ltd. (Beijing, China). Alkaline phosphatase (ALP) and Lyso-Tracker Red were obtained from Yeasen Biotechnology (Shanghai, China). Dulbecco's modified Eagle's medium (DMEM), RPMI Medium 1640 basic and fetal bovine serum (FBS) were obtained from Gibco (Suzhou, China). Anti-γH2AX (phosphor A139) antibody and goat anti-rabbit IgG H&L (Alexa Fluor® 488) antibody were obtained from Abcam (Shanghai, China). PARP rabbit mAb, cleaved PARP (Asp214) rabbit mAb and caspase 3 rabbit antibody were purchased from Cell Signaling Technology (Shanghai, China). Anti-acetyl histone H3 and anti-acetyl histone H4 (Lys 8) antibodies were provided by Millipore (Billerica, USA). β-Actin Mouse mAb and peroxidase-conjugated affinipure goat anti-mouse/rabbit IgG (H + L) were bought from Proteintech Group Inc. (Wuhan, China). FITC Annexin V apoptosis detection kit was purchased from BD Pharmingen (San Diego, CA, USA). Dynasore was purchased from TCI Development Co., Ltd. (Shanghai, China).

2.2. *Synthesis of **1P** and **2P***

1P was synthesized by standard solid phase peptide synthesis (SPPS) according to the previous literature[38]. To synthesize **2P**, the β-alanine conjugated NBD-Cl was prepared first. Specifically, β-alanine (535 mg) and K_2CO_3 (1.38 g) were dissolved in 40 mL water with constant stirring. NBD-Cl (1 g) was dissolved in 25 mL of methanol, and the solution was then slowly added dropwise to the solution of β-alanine at room temperature. The reaction would be complete in 5 h. After that, the methanol in the reaction solution was removed by vacuum, and the pH of the remaining solution was adjusted to 2.0 with 2 mol/L hydrochloric acid (HCl). The resulting NBD–NH $(CH_2)_2$COOH was directly used in SPPS to make **2P**. **1P** and **2P** were purified by high-performance liquid chromatography (HPLC) and confirmed by time-of-flight mass spectrometry (TOF-MS).

2.3. *ALP mediated self-assembly of **1P** and **2P***

1P/2P solution (4 mmol/L) was prepared by dissolving 4 mg of **1P/2P** in 1 mL PBS with pH value adjusted to 7.4 using Na_2CO_3 solution. To prepare pre-assembled control (**1P/2P** + ALP), 10 U ALP was added into the **1P/2P** solution (4 mmol/L), resulting in **1P/2P** hydrogel a few minutes. Lower concentrations of pre-assembled **1P/2P** + ALP which were used in the cellular experiments were obtained by diluting **1P/2P** hydrogel.

2.4. Time-dependent dephosphorylation

The time-dependent dephosphorylation measurement of **1P** was conducted at 4 °C *in vitro*. Different amounts of ALP were added to **1P** solution (100 μL, 4 mmol/L), individually, to a final ALP concentration of 1, 3 and 10 U/mL. The dephosphorylation process was immediately triggered by ALP. To stop the dephosphorylation process, methanol (500 μL) was added into the mixture at different time points (5, 10, 20, 30 and 60 min). All samples were tested by LC–MS.

2.5. Colony formation assay

HeLa and A549 cells in the logarithmic growth phase were seeded into six-well plates at a density of 1×10^3 cells per well and incubated for 24 h, respectively. The culture medium in every well was replaced with fresh medium w/o different drugs for another 12 h incubation. Fresh medium was added before radio exposure to 2, 4 and 6 Gy of γ-rays (^{137}Cs, with the energy of 662 keV and activity of 3600 Ci). Cell clones, showing up on the next 7−9 days, were stained with 0.25% crystal violet solution for 30 min. After being washed with water, the samples were dried in air. The cell clones were optically imaged and counted for further Sensitizer Enhancement Ratio (SER) analysis according to previous reports[39]. Three parallel experiments were performed in the colony formation assay.

2.6. DNA breakage detection

The DNA damage caused by γ-rays was estimated by comet assay and immunofluorescence staining of γH2AX. Briefly, cells were seeded into confocal cell culture dishes at the density of 2×10^5/dish and incubated for 24 h to allow attachment. The medium in the confocal dishes was replaced with fresh medium containing 10 μmol/L of **1P** (or **1P** + ALP), and incubated at 37 °C for another 12 h. After being replaced with fresh medium, cells were exposed to 6 Gy of γ-rays. This cell treatment process (until the end of the irradiation) was also applied for the following experiments, and the cells were marked as "pretreated cells".

For comet assay, after being washed with ice-cold PBS three times, the pretreated cells were immediately collected in ice-cold PBS at the density of 1×10^6/mL, and stored at 4 °C. The frosted microscope slides were all covered with normal-melting-point agarose. After the solidification, 30 μL of cells resuspension and 70 μL of prewarmed (37 °C) low-melting-point agarose were mixed and added on the slide. After the solidification, the slides were placed in the cold lysed buffer at 4 °C for 2.5 h. After being rinsed with PBS, the slides were then placed in the electrophoretic buffer for 20 min and electrophoresis at 30 V at 4 °C for another 20 min, followed by being rinsed with PBS. Then the slides were neutralized in the neutralizing buffer for 20 min at 4 °C, followed by being washed with PBS. Subsequently, the comets on the slides were stained with ethidium bromide solution (1:400) and observed by fluorescence microscope. The degree of DNA damage was quantified by the percentage of tail DNA, which was analyzed by using comet assay software project (CASP). For γH2AX immunofluorescence analysis, 500 μL anti-γH2AX (phosphor A139) antibody (1:500, Abcam) was used. The staining was visualized and imaged by using the CLSM (Nikon, C2).

2.7. Statistical analysis

The experimental data were statistically analyzed by SPSS 19.0 software (Chicago, USA). The data were expressed in the form of mean ± standard deviation (SD). The comparison between groups was performed by ANOVA analysis. The two comparisons were performed using Student's *t*-test, $P < 0.05$ was considered statistically significant.

3. Results and discussion

3.1. Synthesis and characterization of *1P* and *2P*

After generating the tumor-selective self-assembling peptide HDACI (Nap-G^{D}F^{D}FpYSV, **1P**), we evaluated its potential as a radiosensitizer. To image the ALP-instructed assembly of **1P** in cell culture, 7-nitro-1,2,3-benzoxadiazole (NBD) is used as an N-terminal capping group for the synthesis of NBD-^{D}F^{D}FpYSV (**2P**, shown in Scheme 1A and Supporting Information Fig. S1). NBD motif shows none or weak fluorescence in aqueous solution, but its fluorescence is greatly enhanced in a hydrophobic environment such as in assembled state[40]. Coupling β-alanine with NBD-Cl resulted in NBD–NH$(CH_2)_2$COOH, which was directly used in SPPS to prepare **2P**. **1P** and **2P** were purified by high-performance liquid chromatography (HPLC) and characterized by TOF-MS (Supporting Information Figs. S2 and S3). ALP-instructed morphology conversion of **1P** and **2P** were shown in Fig. 1 and Supporting Information Fig. S4. Both **1P** and **2P** are transparent solutions at 4 mmol/L concentration (Fig. 1A and Fig. S4A). After the addition of ALP, the transparent solutions of both **1P** and **2P** turned into hydrogels (Fig. 1B and Fig. S4B). As shown in the transmission electron microscope (TEM) images (Fig. 1B and Fig. S4B), there are entangled nanofibers with diameter of about ~13 nm and length of micrometers in the **1P** hydrogel. There are finer fibers in **2P** hydrogel with a diameter of ~10 nm. The dephosphorylation profile by HPLC shown in Fig. 1C and Supporting Information Fig. S5 suggested that **1P** was dephosphorylated to form **1** after ALP treatment. These results indicate that self-assembly takes place after the dephosphorylation of **1P** and **2P** to form **1** and **2** by ALP.

3.2. In vitro radiosensitization characterization

Colony formation assay was then performed to evaluate the selective radiosensitization efficiency of **1P** on cells with different ALP expression. HeLa and A549 cells were used in the colony formation assay because these two make a good comparison: HeLa cells high express ALP while A549 cells have little ALP[38]. The innocuous concentrations (10 and 20 μmol/L), which were below the critical assembly concentration, were used in this assay based on previous MTT cell viability assay results[38]. To compare the radiosensitization efficiency of *in situ* self-assembly and pre-assembly of **1P**, the pre-assembled group (**1P** + ALP) was prepared by adding ALP into **1P** solution prior to the assay. To clarify, 10 μmol/L of pre-assembled **1P** + ALP was prepared by diluting the more concentrated **1P** hydrogel in order to maintain its nanofiber morphology (Supporting Information Fig. S6). As shown in Fig. 2A, compared with the control group exposed to IR only, both **1P** and **1P** + ALP at 10 μmol/L sensitized the HeLa cells to IR, but clearly, **1P** makes the cells more vulnerable to IR than **1P** + ALP does, with a sensitizer enhancement ratio of 1.433 and 1.150 at 10% cell survival (SER10), respectively. Optical images shown in Fig. 2C and Supporting Information Fig. S7 indicated that, for HeLa cells, *in situ* self-assembled **1P** exhibited better radiosensitization efficiency than the pre-assembled group **1P** + ALP

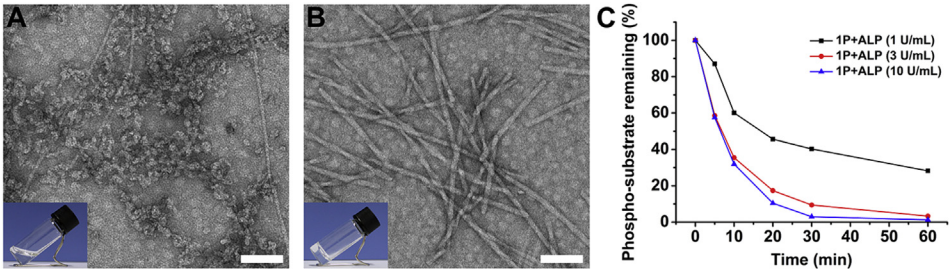

Figure 1 Characterization of ALP-instructed dephosphorylation of **1P**. Optical images (inserts) and TEM images of (A) **1P** and (B) **1P** + ALP. Scale bar = 100 nm. (C) The time-dependent dephosphorylation profile of **1P** (4 mmol/L) in solution after ALP treatment.

did. In contrast, the SER10 value of **1P** in A549 cells with low ALP expression was 0.896 (below 1), even lower than that of **1P** + ALP (1.073, Fig. 2B). This indicated that 10 μmol/L, or even 20 μmol/L of **1P**, did not show any radiosensitizing effect towards A549 cells. When **1P** was catalyzed to form assemblies, it showed a weak sensitizing effect on A549 cells. The SER10 values of **1P** in HeLa cells at concentrations of 5 μmol/L (Supporting Information Figs. S8) and 20 μmol/L (Fig. 2A) were 0.899 and 1.660, respectively, a concentration-dependent manner. These results demonstrated that **1P** significantly enhanced the sensitivity of HeLa cells to γ-ray by *in situ* self-assembling into nanofibers in HeLa cells.

3.3. *Mechanism study of radiosensitization*

After confirming the radiosensitization effect of **1P** on HeLa cells, we continued to investigate the mechanism. In radiotherapy, radiation acts to kill cancer cells primarily *via* breaking the double-strand DNA (DSBs)[41]. Here, we first performed the comet assay to detect DNA damage. In the comet assay, the intensity of the comet tail relative to the total intensity reflects the number of DNA breaks. As shown in Fig. 3, under the 6 Gy radiation, IR only caused little DNA damage to HeLa cells. While **1P** + ALP combined IR led to a higher tail DNA percentage (9.84 ± 2.89%), cells treated by **1P** combined IR had the highest amount of damaged dsDNA (12.28 ± 3.39%). In the case of A549 cells, the pre-assembled **1P** + ALP obviously sensitized A549 cells to γ-ray irradiation (9.24 ± 2.12% *versus* 5.06 ± 1.35% for IR only) and there was no significant difference between the tail DNA percentage of **1P** and IR only groups (5.49 ± 1.41% *versus* 5.06 ± 1.35%, Fig. 3). These results confirmed the benefit of *in situ* EISA to improve radiosensitization.

γH2AX has been identified as a sensitive indicator of DNA DSBs caused by IR. Here we confirmed the effect of **1P** on γ-ray irradiation caused DNA damage by γH2AX staining. γH2AX is the phosphorylated histone H2AX, showing up at sites of

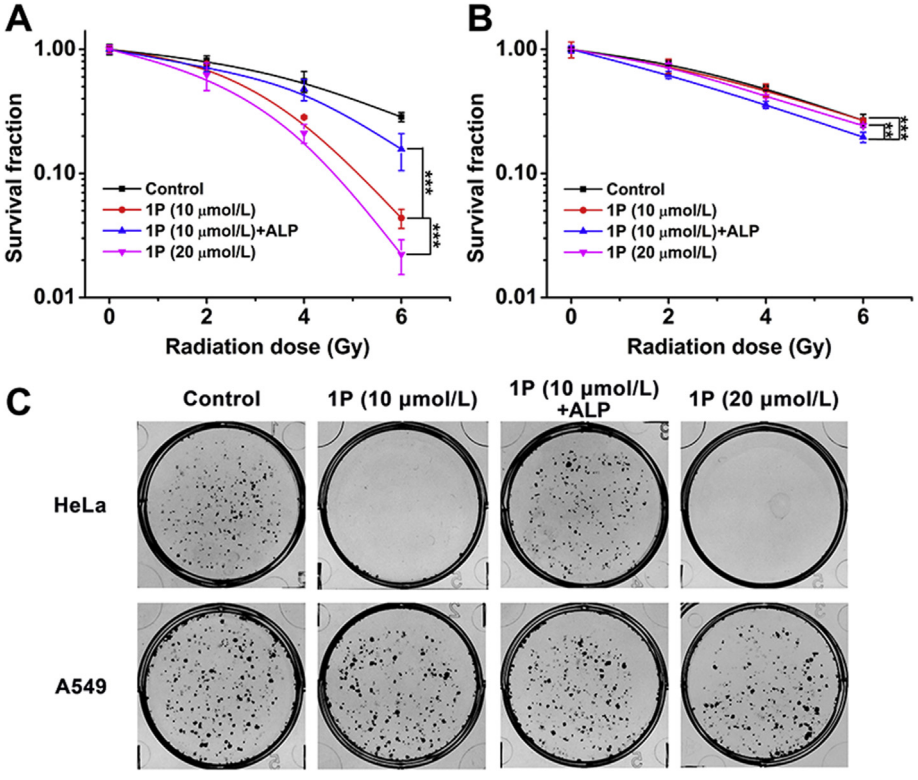

Figure 2 *In vitro* radiosensitization efficiency evaluated by colony formation assay. Colony formation curves of HeLa cells (A) and A549 cells (B) after treatments with **1P** (10 or 20 μmol/L) and **1P** + ALP for 12 h (Data are expressed as mean ± SD, $n = 3$; $^{**}P < 0.01$, $^{***}P < 0.001$). (C) Representative colony formation images of HeLa and A549 cells under 6 Gy of γ-ray irradiation.

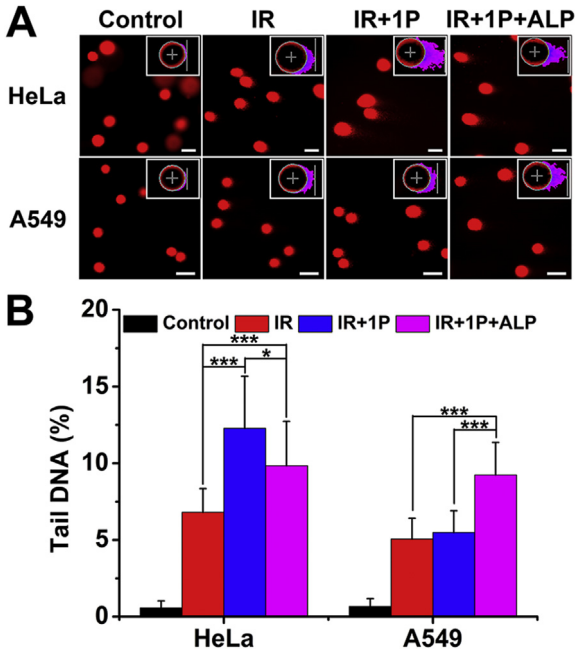

Figure 3 The characterization of DNA damage by comet assay. (A) Comet assay conducted on HeLa and A549 cells exposed to 6 Gy irradiation in the presence of **1P** (10 μmol/L) or **1P** + ALP. Scale bar = 20 μm. Inserts: representative tail DNA image obtained from comet assay software project (CASP). (B) Tailed DNA percentages in HeLa and A549 cells exposed to 6 Gy irradiation in the presence of **1P** or **1P** + ALP (Data are expressed as mean ± SD, $n = 40$; $^{*}P < 0.05$, $^{***}P < 0.001$).

radiation-induced DSBs and becomes visible after immunostaining. The phosphorylation level of histone H2AX was positively correlated with the extent of DSBs[42,43]. As shown in Fig. 4, few γH2AX were present in the HeLa cell nucleus 1 h after irradiation. More γH2AX foci were observed in the cell nucleus in **1P** + ALP combined IR group, suggesting that the DSBs induced by IR were exacerbated by **1P** + ALP. There were even more γH2AX foci in HeLa cells treated with **1P** after IR. Although the γH2AX foci numbers in each group decreased at 3 h after IR, the foci numbers in **1P** combined IR group were still higher than that in other irradiation groups (Supporting Information Fig. S11). Different phenomena were observed in A549 cells. Regardless at 1 or 3 h after IR, **1P** and **1P** + ALP treatments had no significantly different effects on radiation-induced DNA damage (Fig. 4 and Fig. S11). These results aligned with the work done by Yamada and coworkers[44] that HDACIs valproic acid and depsipeptide sensitized tumor cells to radiotherapy by increasing histone H2AX phosphorylation. Although the specific role of γH2AX and its correlation with histone acetylation in radiation-induced DNA damage repair are not clear, these results indicated that **1P** could exert radiosensitizing effects by aggravating the accumulation of DNA DSBs induced by radiation and reducing the repair of DNA damage.

It has been reported that YSV peptide can increase the expression of endogenous cyclin-dependent kinase inhibitors (*e.g.*, p21 and p27) and then suppresses the proliferation of human lung cancer through G0/G1 phase cell cycle arrest[37]. The cell cycle phase determines a cell's relative radiosensitivity, with cells being most radiosensitive in the G2/M phase, less sensitive in the G1 phase and least sensitive during the latter part of the S phase[12,45]. The cell cycle distribution study was performed to investigate whether the cell cycle checkpoints were specifically stimulated by the co-treatments of **1P** and γ-rays (Fig. 5 and Supporting Information Fig. S12). We evaluated the effects of **1P** and **IP** + ALP on the cell cycles of IR-exposed cells. For HeLa cells, the duration of the G2/M phase increased after irradiation, which was consistent with the knowledge that radiation induced cell cycle perturbations and mainly acted on the G2/M phase of cells[46]. It is worth noting that, compared with control and **1P** + ALP groups, **1P** was able to arrest the G1 phase in HeLa cells ($P < 0.001$). While for A549 cells, only the treatment of **1P** + ALP combined with radiation exposure slightly increased cell arrest in the G1 phase ($P < 0.05$, Fig. 5B). The difference in **1P** effects on cell cycles of these two cell lines may explain the different radiosensitivity of cells.

The investigation of cell apoptosis by Annexin V-FITC/PI staining was also performed. The results in Supporting Information Fig. S13 showed that **1P** treatment led to the highest apoptotic ratio (54.27%), as was compared with the irradiation alone (IR, 34.36%) and **1P** + ALP groups (51.86%). Only the pre-assembled **1P** + ALP induced obvious apoptosis in A549 cells. This is consistent with previous results and supported our hypothesis. In HeLa cells with high ALP expression, **1P** is dephosphorylated and

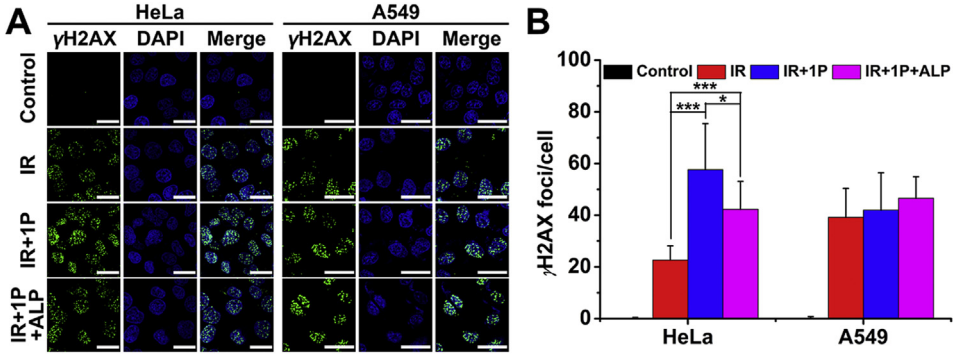

Figure 4 The detection of DNA damage by γH2AX immunofluorescence analysis. (A) Immunofluorescence images of γH2AX in HeLa cells and A549 cells treated with **1P** (10 μmol/L) and **1P** + ALP at 1 h after 6 Gy irradiation. Scale bar = 20 μm. Nuclei were stained with DAPI (blue fluorescence). γH2AX was stained with Alexa Fluor 488 (green fluorescence). (B) Quantization of γH2AX expression in HeLa cells and A549 cells in (A, Data are expressed as mean ± SD, $n = 20$; $^{*}P < 0.05$, $^{***}P < 0.001$).

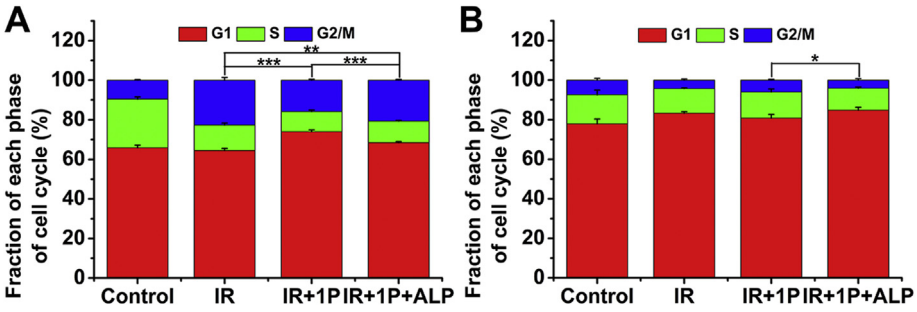

Figure 5 Cell cycle distribution measured by flow cytometry. Cell cycle distribution histograms of HeLa cells (A) and A549 cells (B) treated with **1P** (10 μmol/L) or **1P** + ALP for 12 h w/o 6 Gy irradiation. The cell cycle distribution was detected by flow cytometry 24 h after treatment (Data are expressed as mean ± SD, $n = 3$, and the statistical differences between the groups of G1 phase are shown, $^{*}P < 0.05$, $^{**}P < 0.01$, $^{***}P < 0.001$).

the resulting **1** self-assembled into aggregates. The *in situ* EISA of **1P** had stronger radiosensitizing efficiency than un-assembled and pre-assembled ones.

Caspase 3 and poly (ADP-ribose) polymerase (PARP) levels were also analyzed. PARP is an enzyme involved in DNA repair and plays a critical role in apoptosis[47,48]. As shown in Fig. 6A and B, **1P** treatment upregulated active caspase-3 and PARP in HeLa cells exposed to γ-ray irradiation, suggesting that the exposure to IR in the presence of **1P** led to HeLa cell apoptosis. Our previous studies demonstrated that **1P** at high concentration exhibited HDACI activity and increased the expression of acetylated histone (Ac-H3, and Ac-H4) in HeLa cells[38]. We then studied the effect of **1P** on histone acetylation at low concentration (40 μmol/L). As shown in Fig. 6C and D, **1P** combined with IR treatments significantly upregulated Ac-H3 1.27- and 1.25-fold greater than **1P** and IR alone, respectively. In the case of Ac-H4, it was 1.35 and 1.47 fold, respectively. These results suggested that **1P** at low concentration still had HDAC inhibitory activity and might play a role in the radiosensitizing of HeLa cells.

3.4. *In vitro cellular uptake study*

In order to figure out why the *in-situ* self-assembly of **1P** has a better radiosensitization effect than the pre-assembled **1P** + ALP for HeLa cells, we measured the cellular uptake of the small molecules at different conditions. Here, we use **2P,** an analog of **1P,** which can emit fluorescence and thus is visible. After 4 h incubation, strong green fluorescence from NBD was observed in HeLa cells treated with either **2P** or **2P** + ALP (Fig. 7A). This suggested that ALP expressed on or in HeLa cells could transform **2P** into **2** and turn on the fluorescence of NBD. To our surprise, fluorescence localization and distribution in cells treated with **2P** and **2P** + ALP were completely different. After **2P** + ALP treatment, the intracellular fluorescence in HeLa cells coincided with lysosome fluorescence,

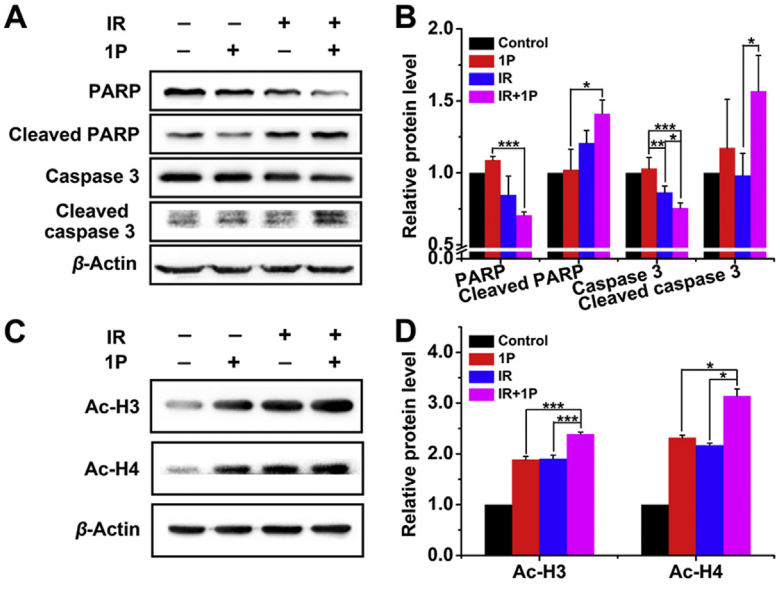

Figure 6 Apoptotic mechanism study by western blotting analysis. (A) Western blot analysis of PARP, Cleaved PARP, Caspase 3 and Cleaved caspase 3 in HeLa cells treated with or without **1P** (40 μmol/L) combined with or without 6 Gy irradiation. β-Actin was used as an internal reference. (B) Quantitative analysis of the expression level of PARP, Cleaved PARP, Caspase 3 and Cleaved caspase 3. (C) Western blot analysis of Ac-H3 and Ac-H4 in HeLa cells treated with or without **1P** (40 μmol/L) combined with or not with 6 Gy irradiation. β-Actin was used as an internal reference. (D) Quantitative analysis of the expression level of Ac-H3 and Ac-H4 (Data are expressed as mean ± SD, $n = 3$; $^{*}P < 0.05$, $^{**}P < 0.01$, $^{***}P < 0.001$).

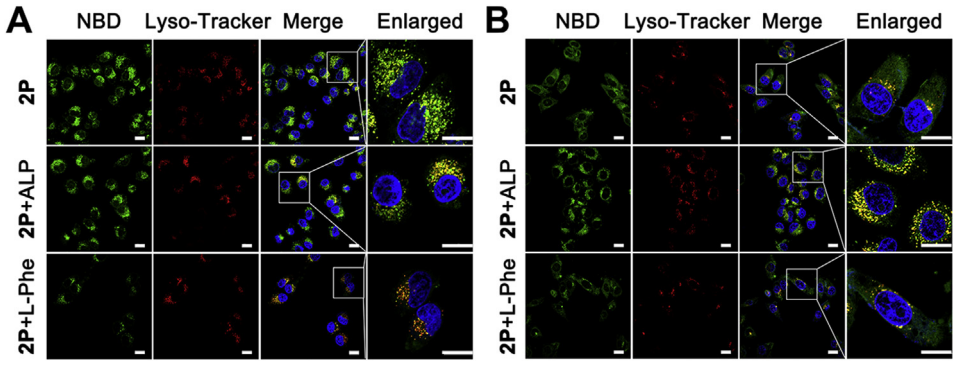

Figure 7 Cellular uptake study. Confocal laser scanning microscopy images of HeLa cells (A) and A549 cells (B) treated with **2P** (50 μmol/L) or **2P** + ALP for 4 h in the absence or presence of the inhibitors L-Phe (100 μmol/L). NBD: green, lyso-tracker: red, DAPI: blue, scale bar = 20 μm.

while after **2P** treatment, only a small part of the fluorescence colocalized with the lysosome and most of them scattered in the cytosol of HeLa cells. A549 cells treated with **2P** + ALP showed a stronger fluorescence than those treated by **2P** and most of them were seen in lysosomes (Fig. 7B). These results indicated that **2P** + ALP, which presented a nanofibrous structure, entered cells through an endocytosis-lysosome pathway. There was apparently weaker fluorescence in A549 cells after 4 h **2P** treatment, agreeing with the fact that A549 cells express less ALPs.

Considering that ALP is highly expressed in and on HeLa cells, L-phenylalanine (L-Phe, an efficient uncompetitive inhibitor for ALP)[49,50] was used to block the EISA and disrupt the formation of fluorescent nanofibers on and in HeLa cells. As is expected, the addition of L-Phe significantly decreased the fluorescence in the HeLa cells treated by **2P**, and the weak fluorescent puncta largely colocalized with lysosomes. Based on all of these results, we speculated that pre-assembled **2P** + ALP entered cells mainly through endocytosis and then escaped from the lysosome to exert their effect. In the case of **2P**, part of them was converted to **2** by ALP on HeLa cell surface, and then self-assembled into nanofibers that were taken up by HeLa cells through endocytosis, while most of **2P** diffused into cells, and *in-situ* assembled into nanofibers catalyzed by intracellular ALP.

From the flow cytometry results and CLSM images shown in Fig. 8A and Supporting Information Fig. S14, we could tell that the fluorescence in both HeLa and A549 cells incubated with **2P** + ALP decreased significantly with the treatment of dynasore, a dynamin-dependent endocytosis inhibitor[51]. This indicated that **2P** + ALP entered cells mainly through dynamin-dependent endocytosis. Notably, compared with HeLa cells treated with **2P**, cells exhibited slightly weak fluorescence after the addition of dynasore, suggesting that endocytosis was not the main pathway for **2P** to enter cells. To further examine the distribution of **2P** in HeLa cells, we build up a 3D reconstruction of the CLSM images. As shown in Fig. 8B, part of the green fluorescent dots from NBD colocalized with the red dots from lyso-tracker, while the addition of dynasore resulted in less fluorescence overlap, confirming that **2P** may diffuse into cells and *in situ* assemble into fluorescent nanoaggregates under the catalysis of intracellular ALP. We reasoned that the resulting nano-assemblies then acted as HDACI, radiosensitizing the cells. There is a completely different situation for the pre-assembled **2P** + ALP. We believed that the pre-formed nanofibers entered cells through the dynamin-dependent endocytosis pathway so most of the nanofibers showed up in lysosomes. Although the mechanism of lysosomal escaping remains unclear, the harsh environment in lysosomes will not be beneficial to peptides, which may weaken their role as HDACI[52]. In addition to avoiding the harsh environment of lysosome, another advantage of *in situ* self-assembly of small molecules inside cells is that it

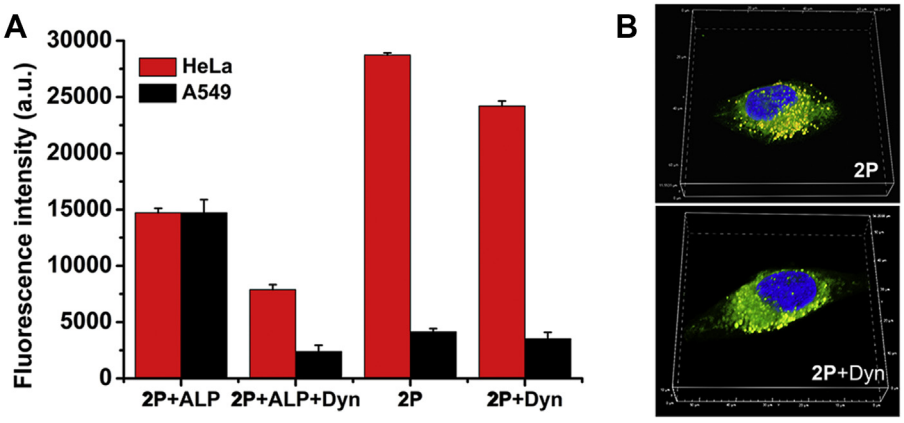

Figure 8 Endocytosis mechanism study by endocytosis inhibitor. (A) Fluorescence quantitative analysis of HeLa and A549 cells treated with **2P** (50 μmol/L) or **2P** + ALP for 4 h with or without dynasore (80 μmol/L) by flow cytometry. (B) 3D images of HeLa cells upon treatment of **2P** (50 μmol/L) for 4 h with or without dynasore (80 μmol/L). NBD: green, lyso-tracker: red, DAPI: blue.

selectively increases the intracellular aggregation of small molecules and reduces the diffusion of small molecules out of cells.

4. Conclusions

In conclusion, we developed a novel radiosensitizer based on the *in situ* EISA of an HDACI peptide derivative. This peptide derivative could selectively sensitize HeLa cells to γ-ray irradiation by accelerating DNA damage, trapping cells in the G1 phase and activating apoptosis. Our work demonstrates that the intracellular *in situ* assembly of small molecules shows great advantages over pre-assembled aggregates as tumor radiosensitizers. That is because the *in situ* EISA of this precursor allows the selective accumulation of HDACI containing nanofibers in cancer cells with high ALP expression, and thus guarantees a better selectivity. This work presents a potential approach to protect drug from degradation in lysosomes and to reduce the escape of small molecules from cells. We believe that this work will lead to a paradigm shift in the treatment of a variety of diseases.

Acknowledgments

This work was supported by the National Natural Science Foundation of China (81971733, 31771085 and 81722026), the CAMS Innovation Fund for Medical Sciences (CIFMS, 2016-I2M-3−022, China), the Non-profit Central Research Institute Fund of Chinese Academy of Medical Sciences (2018RC350016 and 2018PT35031, China) and the Science Foundation for Distinguished Young Scholars of Tianjin (18JCJQJC47300 and 19JCJQJC62200, China).

Author contributions

Jianfeng Liu, Cuihong Yang and Chunhua Ren designed the research. Yang Gao and Jie Gao carried out the experiments and performed data analysis. Ganen Mu, Yumin Zhang and Fan Huang participated part of the experiments. Yang Gao and Cuihong Yang wrote the manuscript. Jianfeng Liu, Chunhua Ren and Wenxue Zhang revised the manuscript. All of the authors have read and approved the final manuscript.

Conflicts of interest

The authors have no conflicts of interest to declare.

Appendix A. Supporting information

Supporting data to this article can be found online at https://doi.org/10.1016/j.apsb.2020.07.022.

References

1. Citrin DE. Recent developments in radiotherapy. *N Engl J Med* 2017;**377**:1065−75.
2. Chen L, Qian M, Jiang H, Zhou Y, Du Y, Yang Y, et al. Multifunctional mesoporous black phosphorus-based nanosheet for enhanced tumor-targeted combined therapy with biodegradation-mediated metastasis inhibition. *Biomaterials* 2020;**236**:119770.
3. Liu JN, Bu W, Shi J. Chemical design and synthesis of functionalized probes for imaging and treating tumor hypoxia. *Chem Rev* 2017;**117**:6160−224.
4. Tang L, Wei F, Wu Y, He Y, Shi L, Xiong F, et al. Role of metabolism in cancer cell radioresistance and radiosensitization methods. *J Exp Clin Canc Res* 2018;**37**:87.
5. Camphausen K, Tofilon PJ. Inhibition of histone deacetylation: a strategy for tumor radiosensitization. *J Clin Oncol* 2007;**25**:4051−6.
6. Wang H, Mu X, He H, Zhang XD. Cancer radiosensitizers. *Trends Pharmacol Sci* 2018;**39**:24−48.
7. Yu CYY, Xu H, Ji S, Kwok RTK, Lam JWY, Li X, et al. Mitochondrion-anchoring photosensitizer with aggregation-induced emission characteristics synergistically boosts the radiosensitivity of cancer cells to ionizing radiation. *Adv Mater* 2017;**29**:1606167.
8. Wang Y, Liu J, Ma X, Liang XJ. Nanomaterial-assisted sensitization of oncotherapy. *Nano Res* 2018;**11**:2932−50.
9. Ni X, Zhang X, Duan X, Zheng HL, Xue XS, Ding D. Near-infrared afterglow luminescent aggregation-induced emission dots with ultrahigh tumor-to-liver signal ratio for promoted image-guided cancer surgery. *Nano Lett* 2019;**19**:318−30.
10. Zhang Y, Huang F, Ren C, Liu J, Yang L, Chen S, et al. Enhanced radiosensitization by gold nanoparticles with acid-triggered aggregation in cancer radiotherapy. *Adv Sci* 2019;**6**:1801806.
11. Tang W, Dong Z, Zhang R, Yi X, Yang K, Jin M, et al. Multifunctional two-dimensional core−shell mxene@ gold nanocomposites for enhanced photo-radio combined therapy in the second biological window. *ACS Nano* 2018;**13**:284−94.
12. Xie J, Gong L, Zhu S, Yong Y, Gu Z, Zhao Y. Emerging strategies of nanomaterial-mediated tumor radiosensitization. *Adv Mater* 2019;**31**:1802244.
13. [Internet] *ClinicalTrials.gov*. Bethesda (MD): U.S. National Library of Medicine; 2002−2020 [cited 2020 Mar 22]. Available from: https://clinicaltrials.gov/ct2/results?cond=radiotherapy&term=nanop article&cntry.
14. Moding EJ, Kastan MB, Kirsch DG. Strategies for optimizing the response of cancer and normal tissues to radiation. *Nat Rev Drug Discov* 2013;**12**:526−42.
15. Zhang C, Wu W, Li RQ, Qiu WX, Zhuang ZN, Cheng SX, et al. Peptide-based multifunctional nanomaterials for tumor imaging and therapy. *Adv Funct Mater* 2018;**28**:1804492.
16. Yang C, Li D, Liu Z, Hong G, Zhang J, Kong D, et al. Responsive small molecular hydrogels based on adamantane-peptides for cell culture. *J Phys Chem B* 2012;**116**:633−8.
17. Yang C, Chu L, Zhang Y, Shi Y, Liu J, Liu Q, et al. Dynamic biostability, biodistribution, and toxicity of L/D-peptide-based supramolecular nanofibers. *ACS Appl Mater Interfaces* 2015;**7**:2735−44.
18. Xu H, Wang T, Yang C, Li X, Liu G, Yang Z, et al. Supramolecular nanofibers of curcumin for highly amplified radiosensitization of colorectal cancers to ionizing radiation. *Adv Funct Mater* 2018;**28**:1707140.
19. Du W, Hu X, Wei W, Liang G. Intracellular peptide self-assembly: a biomimetic approach for *in situ* nanodrug preparation. *Bioconjugate Chem* 2018;**29**:826−37.
20. Zhou J, Xu B. Enzyme-instructed self-assembly: a multistep process for potential cancer therapy. *Bioconjugate Chem* 2015;**26**:987−99.
21. Lin YX, Wang Y, Qiao SL, An HW, Wang J, Ma Y, et al. "*In vivo* self-assembled" nanoprobes for optimizing autophagy-mediated chemotherapy. *Biomaterials* 2017;**141**:199−209.
22. Yang C, Ren C, Zhou J, Liu J, Zhang Y, Huang F, et al. Dual fluorescent- and isotopic- labelled self-assembling vancomycin for *in vivo* imaging of bacterial infections. *Angew Chem Int Ed Engl* 2017;**56**:2356−60.
23. Ye D, Shuhendler AJ, Cui L, Tong L, Tee SS, Tikhomirov G, et al. Bioorthogonal cyclization-mediated *in situ* self-assembly of small-molecule probes for imaging caspase activity *in vivo*. *Nat Chem* 2014;**6**:519−26.
24. Han A, Wang H, Kwok RTK, Ji S, Li J, Kong D, et al. Peptide-induced AIEgen self-assembly: a new strategy to realize highly sensitive fluorescent light-up probes. *Anal Chem* 2016;**88**:3872−8.
25. Lin YX, Qiao SL, Wang Y, Zhang RX, An HW, Ma Y, et al. An *in situ* intracellular self-assembly strategy for quantitatively and temporally monitoring autophagy. *ACS Nano* 2017;**11**:1826−39.

26. Qi GB, Gao YJ, Wang L, Wang H. Self-assembled peptide-based nanomaterials for biomedical imaging and therapy. *Adv Mater* 2018;**30**:1703444.
27. Marks PA, Rifkind RA, Richon VM, Breslow R, Miller T, Kelly WK. Histone deacetylases and cancer: causes and therapies. *Nat Rev Canc* 2001;**1**:194−202.
28. Chen D, Shen A, Fang G, Liu H, Zhang M, Tang S, et al. Tetrahydroisoquinolines as novel histone deacetylase inhibitors for treatment of cancer. *Acta Pharm Sin B* 2016;**6**:93−9.
29. Chen CP, Chen K, Feng Z, Wen X, Sun H. Synergistic antitumor activity of artesunate and HDAC inhibitors through elevating heme synthesis *via* synergistic upregulation of ALAS1 expression. *Acta Pharm Sin B* 2019;**9**:937−51.
30. Cengiz Seval G, Beksac M. A comparative safety review of histone deacetylase inhibitors for the treatment of myeloma. *Expet Opin Drug Saf* 2019;**18**:563−71.
31. Wolchok JD, Hoos A, O'Day S, Weber JS, Hamid O, Lebbé C, et al. Guidelines for the evaluation of immune therapy activity in solid tumors: immune-related response criteria. *Clin Canc Res* 2009;**15**:7412−20.
32. Acetylation TK. Histone deacetylase inhibitors sensitize prostate cancer. *Canc Res* 2007;**67**:5318−27.
33. Natarajan U, Venkatesan T, Radhakrishnan V, Samuel S, Rathinavelu A. Differential mechanisms of cell death induced by HDAC inhibitor SAHA and MDM2 inhibitor RG7388 in MCF-7 cells. *Cells* 2019;**8**:8.
34. Konsoula Z, Velena A, Lee R, Dritschilo A, Jung M. Histone deacetylase inhibitor: antineoplastic agent and radiation modulator. *Adv Exp Med Biol* 2011;**720**:171−9.
35. Wang EC, Min Y, Palm RC, Fiordalisi JJ, Wagner KT, Hyder N, et al. Nanoparticle formulations of histone deacetylase inhibitors for effective chemoradiotherapy in solid tumors. *Biomaterials* 2015;**51**:208−15.
36. Ren C, Gao Y, Guan Y, Wang Z, Yang L, Gao J, et al. Carrier-free supramolecular hydrogel composed of dual drugs for conquering drug resistance. *ACS Appl Mater Interfaces* 2019;**11**:33706−15.
37. Xu Q, Lu R, Zhu ZF, Lv JQ, Wang LJ, Zhang W, et al. Effects of tyroservatide on histone acetylation in lung carcinoma cells. *Int J Canc* 2011;**128**:460−72.
38. Gao Y, Zhang C, Chang J, Yang C, Liu J, Fan S, et al. Enzyme-instructed self-assembly of a novel histone deacetylase inhibitor with enhanced selectivity and anticancer efficiency. *Biomater Sci* 2019;**7**:1477−85.
39. Yin W, Qiang M, Ke W, Han Y, Mukerabigwi JF, Ge Z. Hypoxia-responsive block copolymer radiosensitizers as anticancer drug nanocarriers for enhanced chemoradiotherapy of bulky solid tumors. *Biomaterials* 2018;**181**:360−71.
40. Ren C, Wang H, Zhang X, Ding D, Wang L, Yang Z. Interfacial self-assembly leads to formation of fluorescent nanoparticles for simultaneous bacterial detection and inhibition. *Chem Commun* 2014;**50**:3473−5.
41. Mladenov E, Magin S, Soni A, Iliakis G. DNA double-strand break repair as determinant of cellular radiosensitivity to killing and target in radiation therapy. *Front Oncol* 2013;**3**:113.
42. Kuo LJ, Yang LX. γ-H2AX-a novel biomarker for DNA double-strand breaks. *In Vivo* 2008;**22**:305−9.
43. Sharma A, Singh K, Almasan A. Histone H2AX phosphorylation: a marker for DNA damage. *Methods Mol Biol* 2012;**920**:613−26.
44. Kawano T, Akiyama M, Agawa-Ohta M, Mikami-Terao Y, Iwase S, Yanagisawa T, et al. Histone deacetylase inhibitors valproic acid and depsipeptide sensitize retinoblastoma cells to radiotherapy by increasing H2AX phosphorylation and p53 acetylation-phosphorylation. *Int J Oncol* 2010;**37**:787−95.
45. Pawlik TM, Keyomarsi K. Role of cell cycle in mediating sensitivity to radiotherapy. *Int J Radiat Oncol Biol Phys* 2004;**59**:928−42.
46. Anbumani S, Mohankumar MN. Gamma radiation induced cell cycle perturbations and DNA damage in *Catla Catla* as measured by flow cytometry. *Ecotoxicol Environ Saf* 2015;**113**:18−22.
47. Li X, Li C, Jin J, Wang J, Huang J, Ma Z, et al. High PARP-1 expression predicts poor survival in acute myeloid leukemia and PARP-1 inhibitor and SAHA-bendamustine hybrid inhibitor combination treatment synergistically enhances anti-tumor effects. *EBioMedicine* 2018;**38**:47−56.
48. Ye Y, Zhang T, Yuan H, Li D, Lou H, Fan P. Mitochondria-targeted lupane triterpenoid derivatives and their selective apoptosis-inducing anticancer mechanisms. *J Med Chem* 2017;**60**:6353−63.
49. Wang H, Feng Z, Wang Y, Zhou R, Yang Z, Xu B. Integrating enzymatic self-assembly and mitochondria targeting for selectively killing cancer cells without acquired drug resistance. *J Am Chem Soc* 2016;**138**:16046−55.
50. Dong L, Miao Q, Hai Z, Yuan Y, Liang G. Enzymatic hydrogelation-induced fluorescence turn-off for sensing alkaline phosphatase *in vitro* and in living cells. *Anal Chem* 2015;**87**:6475−8.
51. Harper CB, Popoff MR, McCluskey A, Robinson PJ, Meunier FA. Targeting membrane trafficking in infection prophylaxis: dynamin inhibitors. *Trends Cell Biol* 2013;**23**:90−101.
52. Wang H, Feng Z, Xu B. Assemblies of peptides in a complex environment and their applications. *Angew Chem Int Ed Engl* 2019;**58**:10423−32.